# Nucleation of stable cylinders from a metastable lamellar phase in a diblock copolymer melt

Robert A. Wickham and An-Chang Shi
*Department of Physics and Astronomy, McMaster University, Hamilton, Ontario L8S 4M1, Canada*

Zhen-Gang Wang
*Division of Chemistry and Chemical Engineering, California Institute of Technology, Pasadena, California 91125*

(Received 17 January 2003; accepted 13 March 2003)

The nucleation of a droplet of stable cylinder phase from a metastable lamellar phase is examined within the single-mode approximation to the mean-field Landau–Brazovskii model for diblock copolymer melts. By employing a variational ansatz for the droplet interfacial profile, an analytic expression for the interfacial free energy of an interface of arbitrary orientation between cylinders and lamellae is found. The interfacial free energy is anisotropic and is lower when the cylinder axis is perpendicular to the interface than when the cylinders lie along the interface. Consequently, the droplet shape computed via the Wulff construction is lens like, being flattened along the axis of the cylinders. The size of the critical droplet and the nucleation barrier are determined within classical nucleation theory. Near the lamellar–cylinder phase boundary, where classical nucleation theory is applicable, critical droplets of size 30–400 cylinders across with aspect ratios of 4–10 and nucleation barriers of $(30-40)k_BT$ are typically found. The general trend is to larger critical droplets, higher aspect ratios, and smaller nucleation barriers as the mean-field critical point is approached. © *2003 American Institute of Physics.* [DOI: 10.1063/1.1572461]

## I. INTRODUCTION

The decay of a metastable state via the thermally activated formation and subsequent growth of droplets of the equilibrium phase is known as nucleation. If the nucleation rate is small, the formation of critical droplets—those droplets large enough to overcome the nucleation barrier and grow—can be considered to be a quasiequilibrium process. In the classical homogeneous nucleation scenario, the critical droplet size and nucleation barrier are determined from a balance between the droplet interfacial and bulk free energies.[1]

Nucleation from a disordered initial state to a disordered final state, as occurs in the liquid–gas transition, has been well studied. The study of nucleation when ordered, periodic phases are present is challenging and has been mainly studied in the materials-science context of crystal growth.[2] However, there is also a large class of soft materials where competing interactions select a microscopic length scale and lead to ordered, periodic microphases.[3] Examples include ferrofluids, thin-film magnetic garnets, Rayleigh–Bénard convection, Langmuir monolayers, and block copolymers. Whether the material is hard or soft, the challenge to modeling nucleation in systems with microstructure arises mainly from the need to incorporate the various length scales into the theory. In the case of block copolymer melts these length scales are the interfacial width between microdomains, the period of the microdomains, the width of the droplet interface, and the critical droplet size. Another complication is that the symmetry of the underlying microstructure will lead to anisotropic droplet interfacial free energies and anisotropic critical droplet shapes. Furthermore, the droplet interfacial structure becomes complicated as the different microdomain symmetries merge into each other.

In this paper we will focus on diblock copolymer melts, whose equilibrium phase behavior is well understood.[4–6] At high temperatures the system is disordered, while at lower temperatures several ordered periodic phases—lamellar, hexagonally packed cylindrical, body-centered-cubic spherical, and gyroid—compete for stability. This understanding of the equilibrium properties of diblock copolymer melts provides a solid foundation on which to study the kinetics. Within the diblock copolymer phase diagram we will study nucleation near the first-order lamellar–cylinder phase boundary following a temperature jump into the cylinder phase. This is the simplest order–order transition to examine, yet it contains all of the challenges and issues mentioned above. The goal of this work is to compute the size and shape of the critical droplet and the free-energy barrier to nucleation for a stable cylinder phase nucleating from a metastable lamellar background in a diblock copolymer melt.

Previous theories for the kinetics of order–order transitions in block copolymers have examined the behavior near the order–order spinodal where, in contrast to nucleation, a particular mode of fluctuation out of the metastable state becomes unstable, and the metastable state transforms uniformly throughout the entire sample into a more stable state.[7–13] The recent successful application of self-consistent field theory to block copolymers relies on efficient reciprocal-space methods for treating ordered, uniform periodic phases.[5,8,9] In nucleation, this uniformity is absent, and this has limited the application of reciprocal-space methods to this problem. Notable recent applications of self-

 

consistent field theory to problems involving nonuniformity are studies of the energetics of kink- and twist-grain boundaries in the lamellar phase of diblock copolymer melts[14,15] and studies of T junctions in the lamellar phase of diblock copolymers, both with and without additional homopolymer.[16] The kinetics of various order–disorder and order–order transitions have been studied numerically in Refs. 17–21. The relatively small three-dimensional system sizes currently accessible numerically make handling the various length scales involved in nucleation a challenge. Thus direct numerical studies generally examine transitions across the entire system at once (i.e., the spinodal regime). It is not clear what role, if any, the kinetic pathways and uniform, periodic intermediate states found in these studies play in the nucleation of compact droplets of one ordered phase in another.

The existing theoretical work focusing on nucleation in polymeric systems considers different systems and situations than the one considered here. Wood and Wang recently examined nucleation in polymer blends using self-consistent field theory.[22] Fredrickson and Binder[23] and later Hohenberg and Swift[24] examined the nucleation of a lamellar phase from an initially disordered phase in melts of symmetric diblock copolymers. While Ref. 23 only considered a spherical droplet, Ref. 24 found that the critical droplet shape should be anisotropic, with the lamellar normal along the long axis of the droplet. Two-dimensional numerical simulations by Nonomura and Ohta have recently examined the dynamics of droplets of lamellae nucleating in a metastable cylinder phase.[25] This is close to the situation considered here, and we will discuss it in more detail later.

Early experimental work by Hajduk *et al.* observed a reversible thermotropic transition between the lamellar and cylinder phase in a polystyrene-poly(ethene-*co*-butene) diblock copolymer.[26] The transition pathway from lamellae to cylinders indicated by their data suggests that they were observing spinodal decomposition rather than nucleation. Sakurai *et al.* examined the reverse transition in poly(styrene-*block*-butadiene-*block*-styrene) triblock copolymers, where a nonequilibrium cylinder phase produced by a selective solvent transforms into a stable lamellar phase upon annealing.[27] It appears that they were also observing spinodal decomposition, although the existence of isolated regions of the metastable cylinder phase in their system is interesting. Floudas *et al.* have studied kinetics of the lamellar-to-cylinder transition in poly(isoprene-*block*-ethylene oxide) where the ethylene oxide block is crystalline in the lamellar phase.[28] This crystallinity, the observed rapidity of the transition, and the lack of specific information about the nuclei limit comparison with the present work. Experimental work that directly addresses nucleation is limited to studies of order–disorder transitions between either the disordered and lamellar phases[29] or, as will be discussed in more detail later, the disordered and the cylinder phases.[30–32] These experiments suggest that there is an incubation time, followed by nucleation of anisotropic droplets of the ordered phase from the disordered phase.

To study the decay of a metastable lamellar state via the nucleation of compact droplets of cylinder phase we employ the Landau–Brazovskii model.[9,33,34] This model is appropriate to systems with a weak modulation of the order parameter, or weak segregation, as occurs in mean-field theory for block copolymers near the mean-field critical point. Other phenomena studied using this model include weak crystallization, the nematic-to-smectic-C transition in liquid crystals,[34] and Rayleigh–Bénard convection.[35] The Landau–Brazovskii free energy can be derived from the many-chain Edwards Hamiltonian for diblock copolymers in the weak segregation limit.[4,36] This important connection allows us to move beyond phenomenology in this study and make specific predictions about the size and shape of the critical droplets and the nucleation barrier.

Although we will employ mean-field theory in this paper, it is well known that in diblock copolymers composition fluctuations are important in the vicinity of the second-order mean-field critical point, actually transforming this critical point into a weak first-order transition.[33,37] Thus, when considering the nucleation of lamellae from disorder in symmetric diblock copolymers it is essential to include fluctuations, as they qualitatively change the picture, creating a weak nucleation barrier where in mean-field theory there is none.[23,24] The present situation is different, since the lamellar–cylinder transition for asymmetric diblock copolymers is already first order in mean-field theory. Thus, while fluctuations may modify the size of the nucleation barrier, they should not qualitatively change the physics, provided the barrier is large. We find below that the nucleation barrier grows as $N^{1/2}$, where $N$ is the copolymer degree of polymerization, indicating that fluctuations will be less important for large $N$, consistent with the predictions of Ref. 37. Nevertheless, we expect mean-field theory to eventually break down as the mean-field critical point is approached and the barrier height decreases. After presenting our results, we will discuss where fluctuations may modify these results, and we will indicate how to extend this mean-field calculation to include fluctuations.

We apply the single-mode approximation, accurate at weak segregation, to the Landau–Brazovskii model, which results in an amplitude model studied previously in different contexts.[25,38–40] Since we will work within the framework of classical homogeneous nucleation theory, a key ingredient in our theory is the droplet interfacial free energy. We compute the interfacial free energy for a planar interface separating coexisting lamellar and cylinder phases from the amplitude model. By using a variational approach, we obtain an analytical expression for the interfacial free energy for interfaces of arbitrary orientation. Previous studies of the interfacial free energy, which were primarily numerical, have examined only selected interfacial geometries in two dimensions.[41] With our results for the interfacial free energy, we can compute the droplet shape from the Wulff construction.[42] The Wulff construction has been used to study the anisotropic droplet shape arising during the disorder-to-lamellar transition in Ref. 24 and more recently in Ref. 43. We then apply our results for the interfacial free energies and droplet shape to calculate the critical droplet size and nucleation barrier from classical homogeneous nucleation theory.

## II. THEORY

### A. Landau–Brazovskii theory

We consider an incompressible melt of $n$ AB diblock copolymers in a volume $V_0$ at a temperature $T$. The total degree of polymerization of the diblock copolymer is $N$. The monomer density is thus $\rho_0 = nN/V_0$. The degree of polymerization of the A block is $f_A N$, where $0 \leqslant f_A \leqslant 1$. We employ the Landau–Brazovskii theory for weak crystallization to study nucleation in this system.[9,33,34] The position-dependent order parameter $\phi(\mathbf{r}_0)$ in this theory is defined as the deviation of the normalized A monomer concentration $\phi_A$ from the uniform state and is given by $\phi(\mathbf{r}_0) = \phi_A(\mathbf{r}_0) - f_A$. The Landau–Brazovskii free energy $F_0$ is an expansion in terms of this order parameter,

$$f_0 \equiv \frac{F_0}{nk_BT} = \frac{1}{V_0}\int d\mathbf{r}_0 \left\{ \frac{\xi_0^2}{8q_0^2}[(\nabla^2 + q_0^2)\phi]^2 + \frac{\tau_0}{2}\phi^2 - \frac{\gamma_0}{3!}\phi^3 + \frac{\lambda_0}{4!}\phi^4 \right\}. \tag{2.1}$$

In Eq. (2.1), $f_0$ is the Landau–Brazovskii free energy per block copolymer in units of $k_BT$, $\xi_0$ is the bare correlation length, $q_0$ is the critical wave vector, $\tau_0$ is the reduced temperature, and $\gamma_0$ and $\lambda_0$ are expansion coefficients. For stability, $\lambda_0 > 0$. The Landau–Brazovskii free energy is able to account for the observed diblock copolymer microstructures.[9]

The Landau–Brazovskii free energy can be derived from the many-chain Edwards Hamiltonian for diblock copolymers following the method of Leibler[4] and Ohta and Kawasaki.[36] Like many authors, we have assumed that the third- and fourth-order expansion coefficients are local. The truncation of the order-parameter expansion at fourth order in Eq. (2.1) and the assumption of a single dominant wave vector $q_0$ in the gradient term are valid if the system is in the weak-segregation limit near the mean-field disorder-to-order spinodal and the mean-field critical point. Since, in mean-field theory, a direct lamellar-to-cylinder transition occurs in this region, the Landau–Brazovskii free energy is appropriate to study this transition.

It is convenient to rescale Eq. (2.1) by expressing lengths in units of $q_0^{-1}$ and the free energy is in units of $\lambda_0$. Under the rescalings

$$\mathbf{r} = q_0 \mathbf{r}_0, \tag{2.2}$$

$$V = q_0^3 V_0, \tag{2.3}$$

$$f = \frac{f_0}{\lambda_0}, \tag{2.4}$$

$$\xi^2 = \frac{(q_0\xi_0)^2}{4\lambda_0}, \tag{2.5}$$

$$\tau = \frac{\tau_0}{\lambda_0}, \tag{2.6}$$

$$\gamma = \frac{\gamma_0}{\lambda_0}, \tag{2.7}$$

TABLE I. Mean-field model parameters in the weak-segregation region, from Ref. 37.

| $f_A$ | $x^*$ | $(\chi N)_s$ | $c$ | $N\Gamma_3$ | $N\Gamma_4(0,0)$ |
|---|---|---|---|---|---|
| 0.50 | 3.7852 | 10.495 | 0.4812 | 0.0 | 156.56 |
| 0.45 | 3.7995 | 10.698 | 0.4844 | −8.608 | 169.19 |
| 0.40 | 3.8433 | 11.344 | 0.4945 | −18.81 | 212.22 |

the Landau–Brazovskii free energy becomes

$$f = \frac{1}{V}\int d\mathbf{r}\left\{ \frac{\xi^2}{2}[(\nabla^2+1)\phi]^2 + \frac{\tau}{2}\phi^2 - \frac{\gamma}{3!}\phi^3 + \frac{1}{4!}\phi^4 \right\}. \tag{2.8}$$

One of the goals of this work is to calculate the critical size, shape, and nucleation barrier for droplets of stable cylinder phase nucleating from a metastable lamellar phase in terms of experimentally measurable quantities. To do this we must relate the parameters $q_0$, $\xi_0$, $\tau_0$, $\gamma_0$, and $\lambda_0$ appearing in Eq. (2.1) to such quantities. By following the derivation of Eq. (2.1) in Ref. 36, we can express these parameters in terms of $\chi$, $N$, $f_A$, and $R_g$ that appear in the many-chain Edwards model. Here $\chi$ is the Flory–Huggins interaction parameter characterizing the repulsion between A and B monomers. The diblock copolymer radius of gyration, $R_g$, is defined through

$$R_g^2 = \frac{Nb^2}{6}, \tag{2.9}$$

where $b$ is the Kuhn statistical segment length. We have

$$q_0^2 = \frac{x^*}{R_g^2}, \tag{2.10}$$

$$\xi_0^2 = 4x^* c R_g^2, \tag{2.11}$$

$$\tau_0 = 2[(\chi N)_s - \chi N], \tag{2.12}$$

$$\gamma_0 = -N\Gamma_3, \tag{2.13}$$

$$\lambda_0 = N\Gamma_4(0,0). \tag{2.14}$$

The notation follows that of Leibler.[4] In particular, $x^*$ is the position of the minimum of the function $F(x, f_A)$ appearing in the scattering function of Ref. 4. The disorder-to-order spinodal $(\chi N)_s$ and the quantity $c$ are defined through

$$(\chi N)_s = \tfrac{1}{2}F(x^*, f_A), \tag{2.15}$$

$$c = \frac{1}{2}\left.\frac{d^2F(x,f_A)}{dx^2}\right|_{x=x^*}. \tag{2.16}$$

Finally, the vertex functions $\Gamma_3$ and $\Gamma_4(0,0)$, which are functions of $f_A$, are computed in Ref. 4. In Table I we reproduce the values tabulated by Fredrickson and Helfand for these mean-field parameters in the weak-segregation region.[37] We will take $f_A \leqslant 0.5$ in this paper without loss of generality.

In terms of these parameters, the scaled quantities appearing in Eq. (2.8) are

$$\xi^2 = \frac{(x^*)^2 c}{N\Gamma_4(0,0)}, \tag{2.17}$$

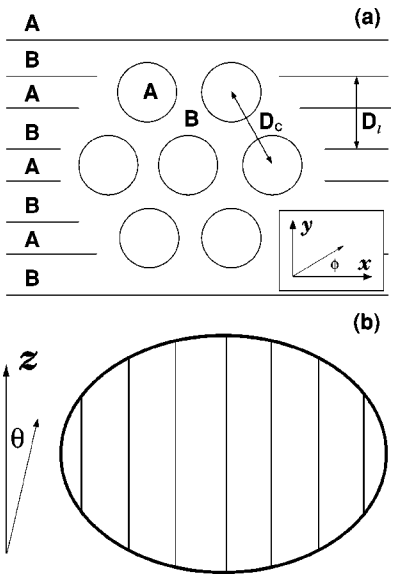


FIG. 1. Schematic picture of the droplet geometry. The critical droplet typically includes many more cylinders than shown. (a) View of the $x-y$ plane. The lamellar normal is along the $y$ axis and the cylinders form a hexagonal lattice inside the droplet with their axes along $z$ (out of the page). The lamellar period is $D_l$: the distance between cylinders is $D_c$. The azimuthal angle $\phi$ is indicated. (b) Perpendicular view to (a), showing the orientation of the cylinders relative to the droplet interface. The polar angle $\theta$ is indicated.

$$\tau = \frac{2[(\chi N)_s - \chi N]}{N\Gamma_4(0,0)}, \tag{2.18}$$

$$\gamma = -\frac{N\Gamma_3}{N\Gamma_4(0,0)}. \tag{2.19}$$

For example, for $f_A = 0.5$ we have $\xi^2 = 0.0440$ and $\gamma = 0$, while for $f_A = 0.45$ we have $\xi^2 = 0.0413$ and $\gamma = 0.0509$. When $\chi N = 11.0$, $\tau = -6.45 \times 10^{-3}$ for $f_A = 0.5$ and $\tau = -3.56 \times 10^{-3}$ for $f_A = 0.45$.

### B. Geometry of the droplet and the single-mode approximation

In principle, to describe a critical droplet of stable cylindrical phase in a background of metastable lamellar phase one needs to find a saddle-point solution to the Euler–Lagrange equations which result from extremizing the free energy, Eq. (2.8). In practice, for the three-dimensional, anisotropic droplets we consider, finding such a solution by a direct numerical method is not, at present, feasible due to the large system sizes required to resolve the various length scales in the problem—the A/B interfacial width, the microstructure period, the droplet interfacial width, and the droplet size. Thus, to make progress, we need to make some basic assumptions about the geometry of the droplet and the form of the order parameter.

We consider a droplet of stable cylindrical phase in a background of metastable lamellar phase with the geometry shown in Fig. 1. Inside the droplet, the cylinders are ordered into a hexagonal lattice and aligned along the $z$ axis. Outside the droplet, the lamellar normal is directed along the $y$ axis. We assume an epitaxial relation between the cylinders and the lamellae. Matsen's work on the cylinder–gyroid and cylinder–sphere transitions shows that these order–order transitions proceed approximately epitaxially and that imposing an epitaxial relation results in only a minor change in the energetics of the transition.[12,13] This suggests that the epitaxial assumption may also have only a slight effect on the energetics of the lamellar–cylinder transition. Experiments on the lamellar-to-cylinder transition,[26,27] which are likely accessing the spinodal regime, and theoretical studies near the spinodal[8,19] indicate that cylinders will form with their axes in the plane of the layers. These results motivate our assumption of this cylinder orientation in the nucleation scenario. The lamellar period $D_l$ is related to $q_0$ by

$$q_0 = \frac{2\pi}{D_l}. \tag{2.20}$$

The distance between cylinders, $D_c$, is epitaxially related to $D_l$ by $D_c = 2D_l/\sqrt{3}$.

The orientational epitaxy enables us to describe both the cylindrical and lamellar orders in terms of a single set of reciprocal-lattice vectors $\mathbf{G}_i$, indexed by the integer $i$. Since we work in the weak-segregation regime, it is sufficient to restrict ourselves to the first mode, those vectors with $|\mathbf{G}_i| = q_0$ (in scaled units, $|\mathbf{G}_i| = 1$), instead of using the complete set of vectors $\mathbf{G}_i$. In the single-mode approximation, the order parameter is written as

$$\phi(\mathbf{r}) = 2a_1(\mathbf{r})\cos(\mathbf{G}_1\cdot\mathbf{r}) + 2a_2(\mathbf{r})[\cos(\mathbf{G}_2\cdot\mathbf{r}) + \cos(\mathbf{G}_3\cdot\mathbf{r})], \tag{2.21}$$

where $a_1$ and $a_2$ are spatially dependent amplitude functions which define the droplet geometry and the $\mathbf{G}_i$ are given (in scaled units) by

$$\mathbf{G}_1 = \hat{\mathbf{y}}, \tag{2.22}$$

$$\mathbf{G}_2 = \tfrac{1}{2}(-\sqrt{3}\hat{\mathbf{x}} + \hat{\mathbf{y}}), \tag{2.23}$$

$$\mathbf{G}_3 = \tfrac{1}{2}(-\sqrt{3}\hat{\mathbf{x}} - \hat{\mathbf{y}}). \tag{2.24}$$

Pure lamellar order is described by $a_1 \neq 0$ and $a_2 = 0$, pure cylindrical order by $a_1 = a_2 \neq 0$.

If we assume the amplitudes $a_1$ and $a_2$ are slowly varying on the scale of $D_c$, we can separate the length scale for variations in the amplitude, the droplet interfacial width, from the length scale of the underlying microstructure. Within this slowly varying amplitude approximation, the Landau–Brazovskii free energy, Eq. (2.8), can be written in terms of the amplitudes as

$$f = \frac{1}{V}\int d\mathbf{r}\{\xi^2(\nabla^2 a_1)^2 + 2\xi^2(\nabla^2 a_2)^2 + 4\xi^2[(\mathbf{G}_1\cdot\nabla a_1)^2 + (\mathbf{G}_2\cdot\nabla a_2)^2 + (\mathbf{G}_3\cdot\nabla a_2)^2] + \tau(a_1^2 + 2a_2^2) - 2\gamma a_1 a_2^2 + \tfrac{1}{4}(a_1^4 + 6a_2^4 + 8a_1^2 a_2^2)\}. \tag{2.25}$$

Extremization of this free energy produces two Euler–Lagrange equations for the amplitudes,

$$2\xi^2\nabla^4 a_1 - 8\xi^2(\mathbf{G}_1\cdot\nabla)^2 a_1 + v_1(a_1,a_2) = 0, \tag{2.26}$$

$$4\xi^2\nabla^4 a_2 - 8\xi^2[(\mathbf{G}_2\cdot\nabla)^2 + (\mathbf{G}_3\cdot\nabla)^2]a_2 + v_2(a_1,a_2) = 0, \tag{2.27}$$

where

$$v_1(a_1,a_2) = 2\tau a_1 - 2\gamma a_2^2 + a_1^3 + 4a_1 a_2^2,$$
$$v_2(a_1,a_2) = 4\tau a_2 - 4\gamma a_1 a_2 + 6a_2^3 + 4a_1^2 a_2. \tag{2.28}$$

The free energy (2.25) and the amplitude equations (2.26) and (2.27) form the basis for our analysis of the droplet nucleation problem.

### C. Equilibrium phase diagram

Lamellar and cylindrical states which are periodic are position-independent solutions of Eqs. (2.26) and (2.27). When $a_1 = a_2 = 0$, the system is disordered. The uniform lamellar solution, which exists for $\tau < 0$, is

$$a_1 = a_l \equiv \sqrt{-2\tau}, \tag{2.29}$$

$$a_2 = 0. \tag{2.30}$$

From Eq. (2.25) we see the uniform lamellar solution has free energy

$$f_l = -\tau^2. \tag{2.31}$$

The uniform cylindrical solution has $a_1 = a_2 = a_c$ with

$$a_c = \frac{\gamma \pm \sqrt{\gamma^2 - 10\tau}}{5} \tag{2.32}$$

and has a free energy

$$f_c = 3\tau a_c^2 - 2\gamma a_c^3 + \tfrac{15}{4} a_c^4. \tag{2.33}$$

For $\gamma > 0$ the solution with the positive root in Eq. (2.32) has the lower free energy and corresponds to cylinders of A in a B matrix. The case for $\gamma < 0$ can be constructed from the $\gamma > 0$ case by recognizing that the free energy, Eq. (2.33), is invariant under $\gamma \to -\gamma$ and $a_c \to -a_c$. It is straightforward to show that, along a phase boundary or spinodal, the relations $\tau = x\gamma^2$ and $a_c = \gamma\tilde{a}_c$ hold for $\gamma$ of either sign, with

$$\tilde{a}_c = \frac{1 + \sqrt{1 - 10x}}{5} \tag{2.34}$$

and $x$ a constant. The lamellar–cylinder phase boundary occurs for

$$x = -\frac{7 + 3\sqrt{6}}{5} = -2.8697, \tag{2.35}$$

as noted in Ref. 38, and the cylinder–disorder phase boundary occurs for $x = 4/45$. The stability limits, or spinodals, for these uniform phases can be found by expanding Eq. (2.25) to second order in deviations from the uniform solution and looking for parameters for which the matrix of partial second derivatives has a negative eigenvalue. The disorder-to-order spinodal is just $\tau = 0$. On increasing temperature (increasing $\tau$, decreasing $\chi N$) the stability limit for the lamellar phase is reached when

$$\tau = -2\gamma^2. \tag{2.36}$$

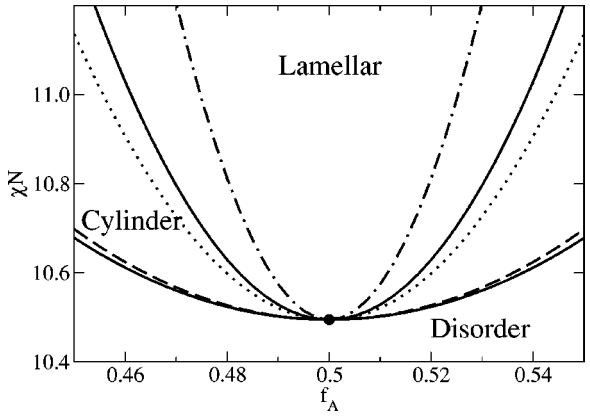


FIG. 2. Equilibrium phase diagram for the Landau–Brazovskii model in the single-mode approximation, Eq. (2.25). The solid lines are phase boundaries between the indicated phases. The dashed line is the disorder-to-order spinodal. The dotted line is the lamellar-to-cylinder spinodal. The dashed-dotted line is the cylinder-to-lamellar spinodal. The body-centered-cubic spherical phase, which is stable between the cylinder and disordered phases, and the gyroid phase, which self-consistent field-theory predicts is stable for $\chi N > 11.14$ along the lamellar–cylinder phase boundary, are not shown. The second-order, mean-field critical point is indicated by the dot.

At this point the lamellar structure will spontaneously transform into the cylinder phase. The spinodal for the reverse, cylinder-to-lamellar, transition occurs when $\tau = -8\gamma^2$.

We construct the equilibrium phase diagram for the free energy, Eq. (2.25), in Fig. 2 in terms of $\chi N$ and $f_A$, using relations (2.18) and (2.19). In mean-field theory there is a second-order critical point at $f_A = 0.5$ and $\chi N = 10.495$ ($\gamma = \tau = 0$), as indicated. In self-consistent field-theory calculations the body-centered-cubic spherical phase is stable between the cylindrical and disordered phases and the gyroid phase is stable along the lamellar–cylinder phase boundary for $\chi N > 11.14$ and $f_A < 0.452$ ($f_A > 0.548$).[5] We have not included these phases in our diagram since our primary concern is with the lamellar–cylinder transition and since we work near the lamellar–cylinder phase boundary for $f_A \geqslant 0.45$. Near the mean-field lamellar–cylinder phase boundary for $0.45 \leqslant f_A \leqslant 0.5$, the free energies of the equilibrium phases calculated from Eq. (2.25) are within a few percent of those obtained from a full self-consistent mean-field calculation,[44] with the difference decreasing as the mean-field critical point is approached. These results indicate the degree of accuracy of the single-mode approximation to the mean-field theory in the region of interest for this study.

### D. Planar interface between the lamellar and cylindrical phases

For a planar interface separating the lamellar and cylindrical phases the amplitudes $a_1$ and $a_2$ become functions of the perpendicular distance to the interface, $s = \hat{\mathbf{n}}\cdot\mathbf{r}$, only. The unit normal to the interface is $\hat{\mathbf{n}} = (\cos\phi\sin\theta, \sin\phi\sin\theta, \cos\theta)$, expressed in terms of the angles defined in Fig. 1. From Eq. (2.25), the free energy per unit interfacial area, $\tilde{f}$, is then

$$\tilde{f}=\int ds\{\xi^2(a_1'')^2+2\xi^2(a_2'')^2+4\xi^2[(\mathbf{G}_1\cdot\hat{\mathbf{n}})^2(a_1')^2 +\{(\mathbf{G}_2\cdot\hat{\mathbf{n}})^2+(\mathbf{G}_3\cdot\hat{\mathbf{n}})^2\}(a_2')^2]+\tau(a_1^2+2a_2^2) -2\gamma a_1a_2^2+\tfrac{1}{4}(a_1^4+6a_2^4+8a_1^2a_2^2)\}, \quad (2.37)$$

where primes denote differentiation with respect to $s$. We note that

$$(\hat{\mathbf{n}}\cdot\mathbf{G}_1)^2=\sin^2\phi\sin^2\theta, \quad (2.38)$$

$$(\hat{\mathbf{n}}\cdot\mathbf{G}_2)^2+(\hat{\mathbf{n}}\cdot\mathbf{G}_3)^2=\tfrac{1}{2}(1+2\cos^2\phi)\sin^2\theta. \quad (2.39)$$

Thus terms involving the squares of single derivatives of the field (square-gradient terms) do not contribute to $\tilde{f}$ when the interface normal is in the $\hat{\mathbf{z}}$ direction ($\theta=0$).

## III. ENERGETICS OF THE LAMELLAR–CYLINDER INTERFACE

The aim of this section is to compute the interfacial free energy for a planar interface of arbitrary orientation $\hat{\mathbf{n}}$ between coexisting epitaxial lamellar and cylindrical phases, aligned as shown in Fig. 1. Once the interfacial free energy is known, the Wulff construction[42] can be used to find the minimal-energy droplet shape, as we show in the next section. It is sufficient to approximate the interfacial free energy near the lamellar–cylinder phase boundary by its value at boundary since the interfacial free energy function is continuous through the transition.

### A. Analytic calculation of the interfacial free energy

Rather than numerically solving the Euler–Lagrange equations resulting from Eq. (2.37) to get the interfacial profile and then computing the interfacial free energy, we instead employ a variational ansatz for the interfacial profile which allows the interfacial free energy to be calculated analytically. Our variational solution to the problem will, of course, produce an interfacial free energy which is greater than that obtained through an exact solution of the Euler–Lagrange equations. However, our analytical solution will give us much insight into the behavior of the interfacial free energy along the lamellar–cylinder phase boundary.

We employ the following variational ansatz for the amplitude profile of a planar interface between coexisting cylinder and lamellar phases,

$$a_1(s)=\left(\frac{a_l+a_c}{2}\right)+\left(\frac{a_l-a_c}{2}\right)h\left(\frac{s}{w}\right), \quad (3.1)$$

$$a_2(s)=\frac{a_c}{2}\left[1-h\left(\frac{s}{w}\right)\right]. \quad (3.2)$$

The function $h$ has the properties that $h(s)\to\pm1$ as $s\to\pm\infty$ and $h(0)=0$; thus it describes a pure cylinder phase for $s\to-\infty$ separated by an interface at $s=0$ from a pure lamellar phase, obtained as $s\to\infty$. The form of $h$ will be specified later. The variational parameter $w$ characterizes the interfacial width and will depend on the interface orientation.

Substitution of Eqs. (3.1) and (3.2) into the free energy, Eq. (2.37), and the rescaling of $s$ to extract factors of $w$ results in the excess free energy due to the interface,

$$\tilde{f}-\tilde{f}_h=\frac{\xi^2\gamma^2g_1}{w^3}+\frac{\xi^2\gamma^2g_2}{w}+\gamma^4g_3w, \quad (3.3)$$

where

$$\tilde{f}_h=\int ds f_l \quad (3.4)$$

is the free energy contribution from the two uniform phases ($f_l=f_c$ at the lamellar–cylinder phase boundary). The coefficients in Eq. (3.3) are

$$g_1=\tfrac{1}{4}I_1(\tilde{a}_l^2-2\tilde{a}_l\tilde{a}_c+3\tilde{a}_c^2), \quad (3.5)$$

$$g_2=\tfrac{1}{2}I_2[3\tilde{a}_c^2+2\tilde{a}_l(\tilde{a}_l-2\tilde{a}_c)\sin^2\phi]\sin^2\theta, \quad (3.6)$$

$$g_3=\int_{-\infty}^{\infty}ds\{x(\tilde{a}_1^2+2\tilde{a}_2^2)-2\tilde{a}_1\tilde{a}_2^2+\tfrac{1}{4}(\tilde{a}_1^4+6\tilde{a}_2^4 +8\tilde{a}_1^2\tilde{a}_2^2)+x^2\}, \quad (3.7)$$

where

$$I_1=\int_{-\infty}^{\infty}ds(h'')^2, \quad (3.8)$$

$$I_2=\int_{-\infty}^{\infty}ds(h')^2. \quad (3.9)$$

The quantity $\tilde{a}_l=\sqrt{-2x}$, and $\tilde{a}_c$ and $x$ are given by Eqs. (2.34) and (2.35). In Eq. (3.7) the functions $\tilde{a}_1$ and $\tilde{a}_2$ are given by Eqs. (3.1) and (3.2) with $a_l$ and $a_c$ replaced by $\tilde{a}_l$ and $\tilde{a}_c$, respectively, and with $w=1$. The coefficients $g_1$, $g_2$, and $g_3$ are positive. The excess free energy, Eq. (3.3), is minimized when

$$w^2=(w^*)^2\equiv\frac{\xi^2g_2+\sqrt{\xi^4g_2^2+12\xi^2\gamma^2g_1g_3}}{2\gamma^2g_3}. \quad (3.10)$$

Substitution of this value for $w$ in Eq. (3.3) provides the interfacial free energy, $\sigma(\theta,\phi)\equiv\tilde{f}^*-\tilde{f}_h$, for a planar cylinder–lamellar interface with normal $\hat{\mathbf{n}}$,

$$\sigma(\theta,\phi)=\frac{\xi^2\gamma^2g_1}{(w^*)^3}+\frac{\xi^2\gamma^2g_2}{w^*}+\gamma^4g_3w^*. \quad (3.11)$$

These results are derived along the lamellar–cylinder phase boundary; thus the temperature ($\tau$) dependence in Eqs. (3.10) and (3.11) enters through $\gamma$ via the relation $\gamma=\sqrt{\tau/x}$, with $x$ given by Eq. (2.35). The limit as $\gamma\to0$ corresponds to approaching the mean-field critical point along the lamellar–cylinder phase boundary. The angular dependence in Eq. (3.11) is contained in $g_2$ and $w^*$. Equation (3.6) indicates that the interfacial free energy depends on the polar angle $\theta$ through factors of $\sin^2\theta$. Equation (3.6) also shows that the interfacial free energy is invariant under $\phi\to\phi+n\pi$, where $n$ is an integer (twofold azimuthal symmetry).

To examine the behavior of $\sigma(\theta,\phi)$ along the phase boundary near the mean-field critical point, we have to distinguish between two cases, depending on the relative values of $\theta$ and $\gamma$. The case where the interface normal is oriented along the $\hat{z}$ direction ($\theta=0$) is special. For orientations away from this special orientation—that is, for $\theta$ nonzero and fixed—we have $|\gamma| \ll g_2$ as the mean-field critical point is approached and obtain the behavior

$$w^* = \frac{\xi}{|\gamma|}\sqrt{\frac{g_2}{g_3}} + O(|\gamma|) \tag{3.12}$$

and

$$\sigma(\theta,\phi) = 2\xi|\gamma|^3\sqrt{g_2 g_3} + O(|\gamma|^5). \tag{3.13}$$

At the mean-field critical point $\gamma \to 0$ and $\xi$ approaches a constant [see Eq. (2.17)]; thus the width of the interface diverges and the interfacial free energy vanishes. It is interesting to note that the interfacial free energy remains anisotropic (via $g_2$) in this limit. Since $\gamma \sim \sqrt{\tau}$ along the phase boundary, the scaling with $\gamma$ seen in Eqs. (3.12) and (3.13) corresponds the mean-field results, $w \sim \tau^{-1/2}$ and $\sigma \sim \tau^{3/2}$ expected near a second-order mean-field critical point.[45]

In the limit $\gamma \to 0$ and $\theta \to 0$ such that $g_2 \ll |\gamma|$ holds we have

$$w^* = \left(\frac{\xi}{|\gamma|}\right)^{1/2}\left(\frac{3g_1}{g_3}\right)^{1/4}\left[1 + \frac{\xi g_2}{2|\gamma|(12 g_1 g_3)^{1/2}} + O\left(\frac{g_2^2}{\gamma^2}\right)\right] \tag{3.14}$$

and

$$\sigma(\theta,\phi) = \tfrac{4}{3}\xi^{1/2}|\gamma|^{7/2}(3 g_1 g_3^3)^{1/4} \times\left[1 + \frac{3\xi g_2}{2|\gamma|(12 g_1 g_3)^{1/2}} + O\left(\frac{g_2^2}{\gamma^2}\right)\right]. \tag{3.15}$$

As $\gamma \to 0$, the condition $g_2 \ll |\gamma|$ restricts the region over which this behavior holds to very small $\theta$, i.e., to interfacial orientations near or at the special orientation. Equations (3.14) and (3.15) show that for these interfacial orientations, the interfacial width diverges more slowly than Eq. (3.12) and the interfacial free energy vanishes more rapidly than Eq. (3.13) as the mean-field critical point is approached. The scaling with $\gamma$ ($\sim\sqrt{\tau}$) seen in Eqs. (3.14) and (3.15) is exactly what mean-field theory predicts for a Lifshitz critical point.[46,47] At a Lifshitz critical point both $\tau$ and the square-gradient terms in the free energy vanish, as occurs here for the free energy, Eq. (2.37), when the interfacial normal is along the $\hat{z}$ direction ($\theta=0$). It is important, however, to emphasize that there is no Lifshitz critical point in the diblock copolymer melt phase diagram since the diblock copolymer melt is a single-component system. In the present case adjusting $\theta$, rather than a thermodynamic state variable, causes the square-gradient terms in the free energy to vanish. We expect that the mean-field critical scaling behavior in Eqs. (3.12)–(3.15) will be modified by fluctuations. For Eqs. (3.14) and (3.15) these modifications may be particularly large, since the upper critical dimension for a Lifshitz critical point is 8. Finally, far from the mean-field critical point, for large $|\gamma|$, the condition $|\gamma| \gg g_2$ holds for all $\theta$ and the expressions (3.14) and (3.15) apply. At leading order $w^* \to 0$ and $\sigma \to \infty$ for large $|\gamma|$. The interfacial free energy becomes isotropic in this limit.

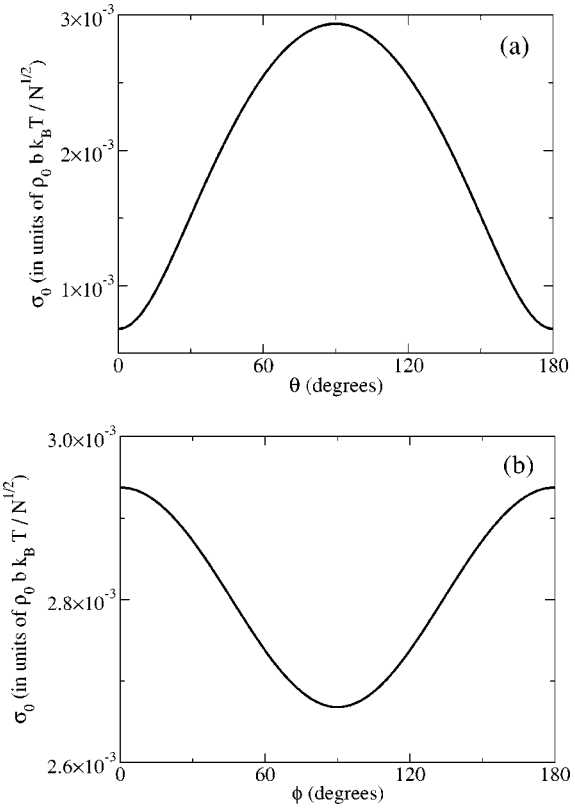


FIG. 3. Interfacial free energy $\sigma_0$ in units of $\rho_0 b k_B T/N^{1/2}$, of the lamellar–cylinder interface at the lamellar–cylinder phase boundary for $f_A=0.45$ ($\chi N=11.3263$) as per Eqs. (3.11) and (3.16). (a) As a function of $\theta$, for $\phi=0$. (b) As a function of $\phi$ for $\theta=\pi/2$ (in the $x$–$y$ plane). The angles $\theta$ and $\phi$ are defined in Fig. 1.

None of these results depend on the form chosen for $h$ in the variational approximation. The only approximation in Eqs. (3.1) and (3.2) is that the interfacial profiles for two different orientations have the same basic shape $h$ and can be scaled onto one another by an orientation-dependent scale factor $w$.

### B. Results for the lamellar–cylinder interfacial free energy

To calculate the interfacial free energy we will now choose $h(s)=\tanh s$, which is a reasonable approximation for an interfacial profile and satisfies the boundary conditions mentioned after Eqs. (3.1) and (3.2). With this choice $I_1 = 16/15$, $I_2 = 4/3$, and $g_3 \approx 0.716\,286$. The unscaled (i.e., actual) interfacial free energy $\sigma_0$ is related to $\sigma$ in Eq. (3.11) by

$$\sigma_0 = \frac{\lambda_0}{\sqrt{6x^*}}\left(\frac{\rho_0 b k_B T}{N^{1/2}}\right)\sigma. \tag{3.16}$$

In Fig. 3 we present results for $\sigma_0$ at the phase boundary, in units of $\rho_0 b k_B T/N^{1/2}$, for $f_A=0.45$. Figure 3 qualitatively represents the features of the interfacial free energy for all $f_A$ near the mean-field critical point. The overall magnitude of

the interfacial free energy increases with stronger segregation. In Fig. 3(a) we show $\sigma_0$ as a function of $\theta$ for $\phi=0$. When the cylinder axis is perpendicular to the interface ($\theta=0$) the interfacial free energy is about 4 times smaller than when the cylinders are parallel to the interface ($\theta=\pi/2$). In Fig. 3(b) the interfacial free energy as a function of $\phi$ in the $x-y$ plane ($\theta=\pi/2$) is shown. The interfacial free energy is highest when the lamellae lie perpendicular to the interface ($\phi=0$) and lowest when the lamellae are parallel to the interface ($\phi=\pi/2$). The variation of the interfacial free energy with $\phi$ is less than its variation with $\theta$, since $2\tilde{a}_l(\tilde{a}_l-2\tilde{a}_c)\ll 3\tilde{a}_c^2$ in Eq. (3.6). Although the interfacial free energies for $\phi=\pi/6$ and $\phi=5\pi/6$ are equal, as they should be, it is somewhat surprising that the presence of cylinder lattice planes at these angles does not produce any features in the interfacial free energy. It may be that at higher segregation, where one has to go beyond the single-mode approximation, the existence of cylinder lattice planes will become manifest in the droplet shape. Similar work by Netz *et al.* examined the lamellar–cylinder interfacial free energy numerically when $\theta=\phi=\pi/2$.[41] They found the mean-field critical scaling $\sigma_0\sim\tau^{3/2}$ near the critical point in their model.

## IV. WULFF CONSTRUCTION OF THE CRITICAL DROPLET

In general, the nucleating droplet of cylindrical phase is not spherical and it is necessary to calculate the droplet shape from the anisotropic interfacial free energy, using the Wulff construction.[42] Once the droplet shape is known, the free energy and size of the critical droplet can be calculated.

### A. Wulff construction for the droplet shape

The droplet shape is found by minimizing the droplet surface free energy, subject to the constraint of constant droplet volume. Thus we minimize the function

$$F_{\text{Wulff}}=S_{\text{drop}}-2\mu V_{\text{drop}}, \tag{4.1}$$

where $\mu$ is a Lagrange multiplier, $V_{\text{drop}}$ is the fixed droplet volume, and

$$S_{\text{drop}}\equiv\int dS\,\sigma(\hat{\mathbf{n}}) \tag{4.2}$$

is the integral of the interfacial free energy, Eq. (3.11), over the droplet surface. Implicit in Eq. (4.1) and in the classical nucleation theory we employ is the assumption that the droplet interface width is negligible compared to the droplet size, so that a separation may be made between the bulk and surface of the droplet. We will show this to be the case *a posteriori*, close to the lamellar–cylinder phase boundary.

The minimization of Eq. (4.1) is performed by choosing, for example, the $x-y$ plane and characterizing the shape of the droplet by the height of the interface, $h_0(\mathbf{x}_\perp)$, above this plane at $\mathbf{x}_\perp=(x,y)$. Minimization then leads to the following formula for the height:[48]

$$\tilde{h}(\tilde{\mathbf{x}}_\perp)=[\tilde{g}(\mathbf{m})+\mathbf{m}\cdot\tilde{\mathbf{x}}_\perp]_{\min\ \mathbf{m}}, \tag{4.3}$$

where

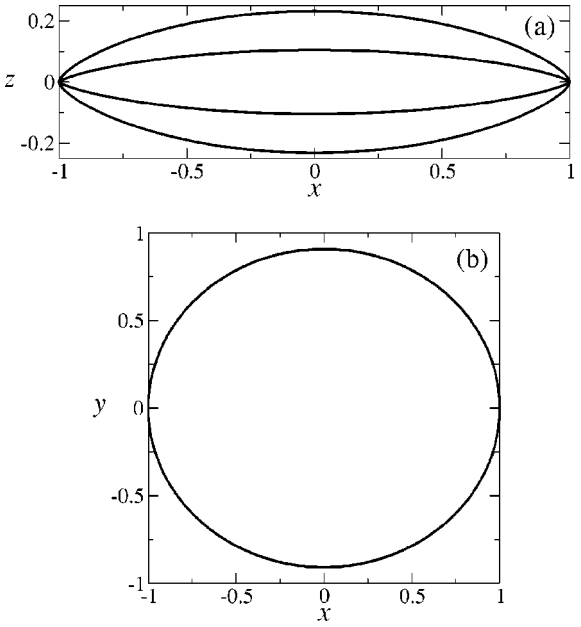


FIG. 4. Cross section of the droplet shape calculated via the Wulff construction. We have chosen the unit of length to be the largest dimension of the droplet, in this case the half-length along the $x$ axis. (a) Cross section in the $x-z$ plane for $f_A=0.45$ (outermost curve) and $f_A=0.49$ (innermost curve) along the lamellar–cylinder phase boundary. The cylinders inside the droplet are oriented along the $z$ axis (vertically) and the lamellae outside the droplet lie in the plane of the page. (b) Cross section in the $x-y$ plane for $f_A=0.45$ and $f_A=0.49$ along the lamellar–cylinder phase boundary. The curves are essentially indistinguishable. The cylinders inside the droplet are in a hexagonal lattice, with their axes pointing out of the page. The lamellae outside the droplet are oriented horizontally, with their normals along the $y$ axis.

$$\tilde{h}=\frac{h_0}{L}, \tag{4.4}$$

$$\tilde{\mathbf{x}}_\perp=\frac{\mathbf{x}_\perp}{L}, \tag{4.5}$$

$$\mathbf{m}=\nabla_\perp h_0, \tag{4.6}$$

$$\tilde{g}(\mathbf{m})=(1+\mathbf{m}^2)^{1/2}\frac{\sigma[\hat{\mathbf{n}}(\mathbf{m})]}{\sigma_{\max}}. \tag{4.7}$$

We have written $\mu=\sigma_{\max}/L$ with $\sigma_{\max}=[\sigma(\hat{\mathbf{n}}(\mathbf{m}))]_{\max\ \mathbf{m}}$ and $L$ a length scale determined by the value chosen for $V_{\text{drop}}$. Equation (4.3) is the essence of the Wulff construction. The minimization in Eq. (4.3) over the variable $\mathbf{m}$ for a given $\tilde{\mathbf{x}}_\perp$ is performed numerically.

The droplet shape along the lamellar–cylinder phase boundary for $f_A=0.45$ and 0.49 is shown in Fig. 4. In this figure we have chosen the unit of length to be the largest dimension of the droplet, in this case the half-length $l_x$ along the $x$ axis. The other dimensions are determined, in these units, through the Wulff construction. Figure 4(a) shows that the droplet is lens-shaped, being flattened along the axis of the cylinders ($z$ axis). This follows from the lower interfacial free energy for interfaces perpendicular to the cylinders, compared to interfaces parallel to the cylinders. The anisotropy of the droplet increases as the mean-field critical point is approached. The droplet shape anisotropy can be charac-

terized by the ratio of $l_x$ to the half-length along the $z$ axis, $l_z$. From Eqs. (4.3) and (4.7) this aspect ratio is

$$\frac{l_x}{l_z}=\frac{\sigma(\pi/2,0)}{\sigma(0,0)}, \tag{4.8}$$

which, from Eqs. (3.13) and (3.15), scales as

$$\frac{l_x}{l_z}\sim \xi^{1/2}|\gamma|^{-1/2}, \tag{4.9}$$

as the critical point is approached, and approaches 1 for large $|\gamma|$. The increase in the aspect ratio of the droplet as the mean-field critical point is approached is a consequence of the fact that the scaling of the interfacial free energy for small $\gamma$ is different in Eq. (3.13) than it is in Eq. (3.15). This difference arises from the vanishing of the square-gradient terms in the free energy when the interfacial normal is oriented along the $\hat{z}$ direction.

Figure 4(b) shows that the droplet is also slightly flattened along the $y$ axis, compared to the $x$ axis. This reflects the trend seen in Fig. 3(b), where the interfacial free energy is lower when the lamellae lie along the interface than when they are perpendicular to it. As expected, the droplet shape anisotropy is weaker in the $x-y$ plane than it is in the $x-z$ plane. The change in the droplet shape anisotropy in the $x-y$ plane with $f_A$ is also very small. If $l_y$ is the half-length of the droplet along the $y$ axis, Eqs. (4.3), (4.7), and (3.13) lead to

$$\frac{l_y}{l_x}=\sqrt{\frac{g_2(\pi/2,\pi/2)}{g_2(\pi/2,0)}}=0.9074, \tag{4.10}$$

at leading order in $|\gamma|$ as the critical point is approached. Thus near the mean-field critical point the droplet will become extremely flattened along the $z$ axis, with a slightly noncircular cross section in the $x-y$ plane. For large $|\gamma|$, Eq. (3.15) indicates that the droplet shape will become isotropic, and $l_y/l_x\to 1$. As anticipated, the presence of cylindrical lattice planes at $\phi=\pi/6$ and $\phi=5\pi/6$ is not manifest in the droplet shape in the $x-y$ plane. We will compare these results for the droplet shape with relevant experimental and numerical results in the Discussion section.

### B. Critical droplet

The droplet volume serves as a reaction coordinate during the transformation from the metastable lamellar phase to the stable cylinder phase. Once this volume is selected, the droplet shape that minimizes the surface free energy is determined from the Wulff construction. We will employ the classical homogeneous nucleation theory,[1] in which the critical droplet corresponds to a total free energy maximum along the volume reaction coordinate and the total free energy is a sum of surface and bulk terms. The computed droplet shape is independent of the value chosen for the droplet volume; thus the shape of the critical droplet will be just as that calculated in the last section.

When we choose the unit of length to be the largest dimension of the droplet, as in the last section, we can compute the droplet volume $V_{\rm drop}$ and surface free energy $S_{\rm drop}$ in these units as functions of $f_A$. When $f_A=0.45$, for example, $S_{\rm drop}=1.949\,57\times10^{-4}$ and $V_{\rm drop}=0.784\,000$ [the interfacial free energy in $S_{\rm drop}$, Eq. (4.2), is dimensionless]. If we wish to express $l_x$ in units of $q_0^{-1}$, the surface free energy $S(l_x)$ and droplet volume $V(l_x)$, in units of $q_0^{-2}$ and $q_0^{-3}$, respectively, will scale as

$$S(l_x)=S_{\rm drop}l_x^2, \tag{4.11}$$

$$V(l_x)=V_{\rm drop}l_x^3, \tag{4.12}$$

for arbitrary $l_x$.

We now examine the system slightly away from the phase boundary, making the standard assumption of classical nucleation theory that the interfacial free energy and interfacial width do not change significantly near the phase boundary. When the lamellar phase is metastable and the cylinder phase is stable we have

$$\Delta f\equiv f_c-f_l<0. \tag{4.13}$$

Separating the free energy $F_0$ (in real free energy units) into a bulk and a surface term and subtracting the free energy $F_l$ of the metastable uniform lamellar phase, we have

$$\frac{(F_0-F_l)N}{\rho_0 k_B T}=\frac{\lambda_0}{q_0^3}[V_{\rm drop}l_x^3\,\Delta f+S_{\rm drop}l_x^2]. \tag{4.14}$$

The critical droplet occurs for the half-length $l_{cx}$ that maximizes this expression, namely,

$$l_{cx}=-\frac{2S_{\rm drop}}{3V_{\rm drop}\Delta f}, \tag{4.15}$$

for which the nucleation barrier $\Delta F_c\equiv F_{\rm crit}-F_l$ is given by

$$\frac{\Delta F_c}{\rho_0 b^3 N^{1/2}k_B T}=\frac{\lambda_0}{(6x^*)^{3/2}}\frac{4(S_{\rm drop})^3}{27(V_{\rm drop})^2(\Delta f)^2}. \tag{4.16}$$

The critical half-length in Eq. (4.15) is expressed in units of $q_0^{-1}$. Equation (2.10) has been used in Eq. (4.16).

In Fig. 5 we plot $\Delta F_c$ in units of $\rho_0 b^3 N^{1/2}k_B T$ near the lamellar–cylinder phase boundary for $f_A=0.45$ and 0.49. The nucleation barrier diverges at the phase boundary, but remains finite at the spinodal—behavior to be expected from classical nucleation theory. Physically, the nucleation barrier should go to zero at the spinodal, but this is beyond the classical nucleation approach employed here. Note that the scale on the vertical axis is smaller in Fig. 5(b) than it is in Fig. 5(a)—in mean-field theory the nucleation barrier vanishes when $f_A=0.5$. The importance of Fig. 5 is that it allows one to calculate the magnitude of the nucleation barrier in units of $k_B T$, once $N$, $\rho_0$, and $b$ are known. Since $\Delta F_c$ scales as $N^{1/2}$, we expect polymers with higher indices of polymerization will have larger nucleation barriers. Finally, in Fig. 5 we plot the nucleation barrier obtained using our theory for the interfacial free energy, but with a spherical droplet shape (dashed curve). In this case $\Delta F_c$ is significantly increased, indicating the importance of using the proper, anisotropic droplet shape for an accurate calculation of the nucleation barrier.

In Fig. 6 we examine the dimensions of the critical droplet, $l_{cx}$ and $l_{cz}$, obtained using Eqs. (4.8) and (4.15), as a function of $\chi N$ near the lamellar–cylinder phase boundary for $f_A=0.45$ and $f_A=0.49$. In this figure the lengths are in units of the cylinder spacing $D_c$. In addition to $l_{cx}$ and $l_{cz}$

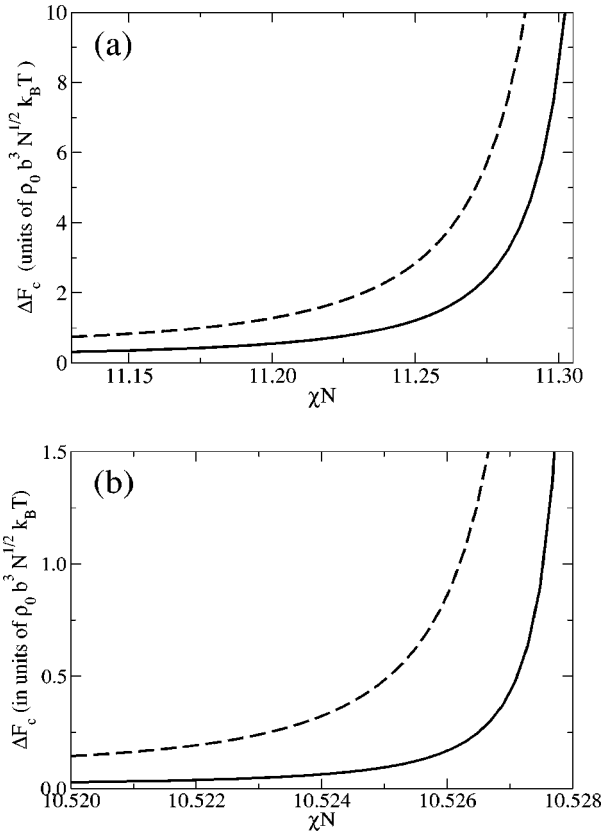


FIG. 5. Nucleation barrier (solid curves) as a function of $\chi N$ near the lamellar–cylinder phase boundary. (a) For $f_A=0.45$, where the phase boundary occurs at $\chi N=11.3263$ and the spinodal occurs at $\chi N=11.1358$. (b) For $f_A=0.49$, where the phase boundary occurs at $\chi N=10.5285$ and the spinodal occurs at $\chi N=10.5207$. For comparison, the dashed curves are the result of using the anisotropic interfacial free energy, Eq. (3.11), but assuming a spherical droplet shape.

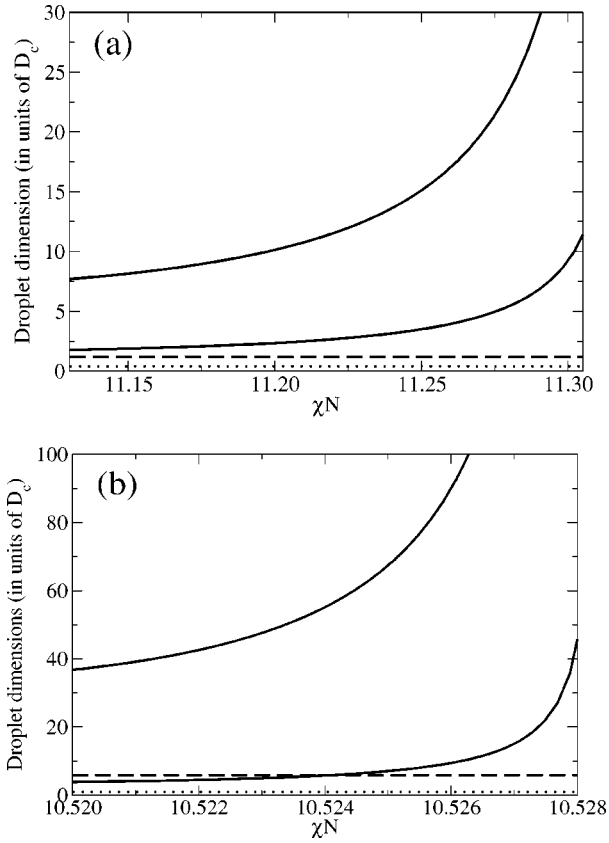


FIG. 6. Critical droplet dimensions, in units of the distance $D_c$ between cylinders, as a function of $\chi N$ near the lamellar–cylinder phase boundary. (a) $f_A=0.45$, (b) $f_A=0.49$. The upper solid curve corresponds to $l_{cx}$, the lower solid curve to $l_{cz}$. The interface widths, calculated at the lamellar–cylinder phase boundary, are indicated: $w_x$ (dashed line), $w_z$ (dotted line). The transitions and spinodals occur in the same places as in Fig. 5.

we also show the droplet interfacial widths $w_x$ and $w_z$, obtained from the calculation of the interfacial free energy at the phase boundary for interfaces oriented with normals along the $x$ and $z$ axes, respectively. The droplet size diverges as the phase boundary is approached, as expected from classical nucleation theory. In Fig. 6 we examine the region in $\chi N$ from the spinodal to the phase boundary. The general trend is for the scale of the critical droplet in this region to increase as the mean-field critical point is approached. As anticipated from Eqs. (3.12) and (3.14) the width of the droplet interface increases as the critical point is approached. Netz *et al.* also observed widening of the lamellar–cylinder interface as the segregation decreased.[41] For these $f_A$ and $\chi N$ we find $l_{cx}>w_x$ and $l_{cz}>w_z$. For $f_A=0.49$ there is a region of $\chi N$ for which $l_{cz}<w_x$. In the next section we will discuss the region of validity of our theory and the range of droplet sizes and nucleation barriers expected in this region.

## V. DISCUSSION

To satisfy the assumptions of the Wulff construction and the classical nucleation theory we study the region close to the lamellar–cylinder phase boundary, but not so close that nucleation is rendered unobservable due to extremely high barriers. In small-molecule binary fluid mixtures, Cahn and Hilliard estimated that a free energy barrier below $60k_BT$ should produce an observable rate of nucleation (at least one nucleation event per day per cubic centimeter, say).[7] Since the relaxational dynamics in polymeric fluids is slower than in small-molecule fluids, we expect that a somewhat smaller free energy barrier is required for nucleation to be observable in our system. However, in the absence of a kinetic theory for nucleation in polymers, we will take $60k_BT$ to be an upper limit for the nucleation barrier. In the context of binary polymer blends, Binder[49] and, more recently, Wang[50] have argued that mean-field theory breaks down when the free energy barrier becomes less than $10k_BT$. Following these authors, we take a nucleation barrier of $10k_BT$ to be the lower limit for applicability of the present theory.

To be consistent with the slowly varying amplitude approximation, the width of the droplet interface should be larger than the microstructure period. For $f_A=0.45$ we have $w_x\approx w_y\approx D_c$, while closer to the mean-field critical point $w_x\approx w_y>D_c$. We typically find $w_z<D_c$ (when $f_A=0.45$, $w_z\approx 0.41D_c$, and it is not until $f_A=0.492$ that $w_z=D_c$). However, since the variations in the underlying microstructure are in the $x-y$ plane, relatively rapid variations of the amplitude in the $z$ direction should not affect the validity of the slowly varying amplitude approximation. For $f_A=0.45$

and $\chi N=11.25$ with $N=1000$ and $\rho_0=b^{-3}$ the nucleation barrier is $39k_BT$ and the critical droplet, which has an aspect ratio of 4.3, is about 30 cylinders across. These numbers are reasonable, so we take $f_A\approx 0.45$ as the lower bound on $f_A$ for which the theory is valid. For $f_A<0.452$ self-consistent field theory predicts that the gyroid phase is stable along the lamellar–cylinder phase boundary. Furthermore, the weak-segregation approximation will become increasingly inaccurate as $f_A$ decreases.

As the mean-field critical point is approached the trend is for the nucleation barrier to decrease, the droplet interface width to increase, and the droplet size to increase. Thus the slowly varying amplitude approximation should be increasingly accurate as the critical point is approached. We also have $l_{cx}>w_x$ and $l_{cz}>w_z$ in this limit, which is a necessary condition for the classical nucleation and Wulff approaches to be valid. It is possible for $l_{cz}<w_x$ for some superheatings, as seen in Fig. 6(b), possibly indicating a breakdown of this approach; however, one can go to smaller superheatings where $l_{cz}>w_x$. As an example, for $f_A=0.49$ and $\chi N=10.5275$ with $N=1000$ and $\rho_0=b^{-3}$, the nucleation barrier is $28k_BT$ and the critical droplet, which has an aspect ratio of about 10, is about 420 cylinders across. For these values of $f_A$ and $\chi N$ we find $l_{cz}\approx 3.7w_x$. The interfacial width for interfaces parallel to the cylinders is on the order of $(5-6)D_c$, while for perpendicular interfaces the width is on the order of $0.9D_c$. Near the mean-field critical point fluctuations will be important and will renormalize the basic model, Eq. (2.1), as discussed in Refs. 33 and 37. The technique discussed here can be applied to study nucleation in the renormalized Landau–Brazovskii model, in which the lamellar–cylinder phase boundary terminates at a lamellar–cylinder–disorder triple point for $f_A<0.5$, where the nucleation barrier is expected to remain finite.[37] We expect that when the nucleation barrier becomes less than about $10k_BT$, near either the mean-field critical point or the mean-field spinodal curve, the distinction between nucleation and spinodal decomposition will be lost and our approach will require modification.

We are not aware of any experimental investigations of the shape and size of nuclei in transitions between the lamellar and cylindrical phases in diblock copolymer melts. However, it is worth noting some experimental observations on related systems. Koizumi *et al.* used transmission electron microscopy to study a blend of poly(styrene-*block*-isoprene) and homopolystyrene, which macrophase separated to form diblock-rich, lens-shaped droplets in a homopolymer-rich matrix.[51] Microphase separation into a hexagonal lattice of cylinders occurred in the droplets, with the cylinder axis aligned along the short axis of the lenslike macrodomain, which had an aspect ratio of about 3.5. Perpendicular to the cylinder orientation, the droplet had an approximately circular cross section of about 20 cylinders in diameter. While their observations closely resemble our results for the critical droplet at $f_A=0.45$, their system is quite different from ours. First, they are looking at macrophase separation, rather than nucleation. Second, in their droplet the cylinders terminate at the interface with the disordered, homopolymer-rich phase, while ours merge continuously into a lamellar structure. Thus, while the relationship, if any, between these experiments and our theory remains to be understood, it is intriguing that droplets similar to those predicted here exist in nature.

Balsara and co-workers have examined the evolution of cylindrical order in poly(styrene-*block*-isoprene) following a quench from the disordered state.[30–32] From their depolarized light-scattering data they inferred that their nuclei had an aspect ratio of about 4 and that nucleation was occurring with the cylinders oriented along the long axis of the droplet. While they observe an anisotropic droplet shape, their cylinders are oriented oppositely to those in the present theory and those in the experiments of Koizumi *et al.*[51] Of course, since the situations studied are all different, it is difficult to draw any conclusions by comparison. However, we have repeated the analysis described here for a droplet of cylinder phase in a metastable disordered background and our preliminary results indicate that the cylinders still align along the short axis of the droplet. Again, the interfacial free energy is lower when the droplet interface lies perpendicular to the cylinder axis. This discrepancy with the conclusions of Refs. 30–32 needs to be better understood.

Nonomura and Ohta recently performed two-dimensional simulations of the nucleation and growth of a droplet of lamellar phase from a metastable cylinder phase.[25] Although this is the reverse of the transition considered here, comparison is possible since the present theory for the interfacial profile and free energy does not refer to which phase is on the inside of the droplet. Their simulations, performed in what here is the $x-y$ plane, observe the epitaxy we assume. Their droplet interface is relatively sharp, with a width on the order of 2–3 cylinder spacings. Their data suggest that the droplet has a hexagonal shape in the the $x-y$ plane, although their larger droplets, on the order of 20 cylinders across, appear more circular. In the absence of a precise definition of the droplet surface in the simulations, these observations about the droplet shape can only be considered qualitative. It appears that the critical droplet size in the simulations is less than 1–2 cylinder spacings, since droplets of all sizes grow. This small critical droplet size, less than that found here, may occur because of different model parameters used in the simulations or because the droplet was nucleated heterogeneously by creating a dislocation pair in the cylindrical order, thereby lowering the barrier to nucleation.

We have demonstrated the crucial connection between anisotropy in the interfacial free energy and droplet shape, and Fig. 5 demonstrates the importance of using the proper critical droplet shape to accurately calculate the nucleation barrier. Thus it is important to consider the robustness of our results for the critical droplet shape and nucleation barrier. We consider the class of models for diblock copolymers where the free energy is written in terms of a Landau expansion in the order parameter and whose gradient structure occurs at quadratic order in the order parameter. This class includes the Landau–Brazovskii model, the Leibler model with local cubic and quartic coefficients,[4] and the Ohta–Kawasaki model.[36] If the single-mode and slowly varying amplitude approximations are applied to this class of models, one can show that the resulting gradient structure will reduce

to that of Eq. (2.25). Since the critical droplet shape depends crucially on the gradient structure of the theory, this suggests, for weak segregation, that the lenslike critical droplet shape calculated here is robust, within mean-field theory. At higher segregations, the presence of higher Fourier modes in the monomer density fields may modify the droplet shape from that calculated here. In particular, we suspect that the low interfacial free energy found when the interface normal is in the $\hat{z}$ direction, due to the vanishing of the square-gradient terms in the free energy, will be modified by the addition of higher Fourier modes. As mentioned earlier, the behavior of the interfacial free energy for this interface orientation may also be strongly affected by fluctuations near the mean-field critical point.

The need to use a variational ansatz to obtain the free energy of a planar interface can be eliminated by solving the amplitude model, Eqs. (2.26) and (2.27), numerically in three dimensions for a droplet of cylinder phase in a background of metastable lamellar phase. Near the phase boundary, we expect no qualitative change in either the droplet shape or the behavior of the nucleation barrier from that reported here. The overall magnitude of the nucleation barrier will, however, be somewhat reduced since the elimination of the variational ansatz will lead to a reduction in the calculated interfacial free energy. This approach will also enable us to go beyond the constraints imposed by the Wulff construction and the classical nucleation theory. It will allow an investigation of the entire metastable lamellar region from the phase boundary to the spinodal. The nucleation barrier should approach zero and the critical droplet dimensions should diverge at the spinodal.[7] As the spinodal is approached and the droplet interface becomes more diffuse the connection between interfacial free energy and droplet shape becomes less clear; thus the droplet shape may be modified near the spinodal. It may be possible to make contact with other theories that address the spinodal limit of order–order transitions.[8–13,19]

In addition to exploring the limits of the theory through the extensions discussed above, we plan to apply the formalism to nucleation at the sphere–cylinder transition. The role of anisotropic fluctuations during this transition has been studied experimentally in Ref. 52. This transition has been studied theoretically in Refs. 8, 13, and 19, assuming uniform intermediate states, but the nucleation of compact droplets has not been examined. Finally, we would like to develop a deeper understanding of the orientation dependence of the interfacial free energy in terms of the structure of the lamellar–cylinder interface and the conformations of block chains at these interfaces.

## VI. CONCLUSION

We have examined the nucleation of a droplet of stable cylinder phase from a metastable lamellar phase using the single-mode approximation to the Brazovskii model for diblock copolymer microphases. By employing a variational ansatz for the droplet interfacial profile, we find an analytic expression for the interfacial free energy of an interface of arbitrary orientation between epitaxially oriented cylinders and lamellae. The interfacial free energy is anisotropic and is lower when the cylinder axis is perpendicular to the interface than when the cylinders lie along the interface. Furthermore, the interfacial free energy is slightly lower when the lamellae are parallel to the interface compared to the perpendicular alignment. The droplet shape computed via the Wulff construction is lenslike, being flattened along the axis of the cylinders. As the mean-field critical point is approached along the lamellar–cylinder phase boundary the droplet becomes more flattened along the cylinder axis. We apply this information to compute the size of the critical droplet and the nucleation barrier within classical nucleation theory. We are able to make specific predictions for these quantities by connecting the phenomenological Landau–Brazovskii model to the many-chain Edwards Hamiltonian for diblock copolymers. The general trend is for the nucleation barrier to decrease and the critical droplet size to increase as the mean-field critical point is approached. The nucleation barrier is significantly reduced when the critical droplet shape is anisotropic instead of spherical, indicating the importance of using the proper droplet shape. The theory should be valid near the lamellar–cylinder phase boundary from the lamellar–gyroid–cylinder triple point at $f_A \approx 0.45$ to near the mean-field critical point. In this regime, droplets of size 30–400 cylinders across with aspect ratios of 4–10 and nucleation barriers of $(30-40)k_BT$ are typically calculated. Close to the mean-field critical point fluctuations may modify this mean-field picture. Due to the variational approximation, the computed interfacial free energies are upper bounds on the true free energies, implying that the computed critical droplet dimensions are also upper bounds on the true dimensions.

This work is an important first step toward a more sophisticated theory of nucleation in this system. The size of the critical droplets we find already suggests that a direct numerical attack on the nucleation problem, using Eq. (2.1), will be challenging. Although our focus has been on nucleation in diblock copolymers, this approach should work for any system in the Landau–Brazovskii class, given the appropriate model parameters. The nucleation scenario described here should be observable experimentally; however, experiments which study droplet nucleation along the lamellar–cylinder phase boundary in diblock copolymer melts have yet to be performed.

## ACKNOWLEDGMENTS

The authors would like to thank Professor Martin Grant for helpful comments. This work was supported by the Natural Sciences and Engineering Research Council of Canada, the Research Corporation, and an Ontario Premier's Research Excellence Award. Z.G.W. acknowledges support by the U.S. National Science Foundation (Grant No. DMR-9970589).

[1] J. S. Langer, in *Systems Far From Equilibrium*, edited by L. Garrido, Lecture Notes in Physics Vol. 132 (Springer, New York, 1980).
[2] S. E. Offerman, N. H. van Dijk, J. Sietsma, S. Grigull, E. M. Lauridsen, L. Margulies, H. F. Poulsen, M. Th. Rekveldt, and S. van der Zwaag, Science (Washington, D.C., U.S.) **298**, 1003 (2002); L.-Q. Chen, Annu. Rev. Mater. Sci. **32**, 113 (2002), and references therein.
[3] M. Seul and D. Andelman, Science (Washington, D.C., U.S.) **267**, 476 (1995).

[4] L. Leibler, Macromolecules **13**, 1602 (1980).
[5] M. W. Matsen and M. Schick, Phys. Rev. Lett. **72**, 2660 (1994).
[6] M. W. Matsen, J. Phys.: Condens. Matter **14**, R21 (2002).
[7] J. W. Cahn and J. E. Hilliard, J. Chem. Phys. **31**, 688 (1959).
[8] C. Yeung, A.-C. Shi, J. Noolandi, and R. C. Desai, Macromol. Theory Simul. **5**, 291 (1996); M. Laradji, A.-C. Shi, R. C. Desai, and J. Noolandi, Phys. Rev. Lett. **78**, 2577 (1997); M. Laradji, A.-C. Shi, J. Noolandi, and R. C. Desai, Macromolecules **30**, 3242 (1997).
[9] A.-C. Shi, J. Phys.: Condens. Matter **11**, 10183 (1999).
[10] S. Qi and Z.-G. Wang, Macromolecules **30**, 4491 (1997).
[11] S. Qi and Z.-G. Wang, Polymer **39**, 4639 (1998).
[12] M. W. Matsen, Phys. Rev. Lett. **80**, 4470 (1998).
[13] M. W. Matsen, J. Chem. Phys. **144**, 8165 (2001).
[14] M. W. Matsen, J. Chem. Phys. **107**, 8110 (1997).
[15] D. Duque and M. Schick, J. Chem. Phys. **113**, 5525 (2000).
[16] D. Duque, K. Katsov, and M. Schick, J. Chem. Phys. **117**, 10315 (2002).
[17] M. Bahiana and Y. Oono, Phys. Rev. A **41**, 6763 (1990).
[18] C. Roland and R. C. Desai, Phys. Rev. B **42**, 6658 (1990); C. Sagui and R. C. Desai, Phys. Rev. Lett. **71**, 3995 (1993); Phys. Rev. E **49**, 2225 (1994); **52**, 2807 (1995); **52**, 2822 (1995); Phys. Rev. Lett. **74**, 1119 (1995).
[19] S. Qi and Z.-G. Wang, Phys. Rev. Lett. **76**, 1679 (1996); Phys. Rev. E **55**, 1682 (1997).
[20] D. Boyer and J. Vinals, Phys. Rev. E **63**, 061704 (2001); Phys. Rev. Lett. **89**, 055501 (2002); Phys. Rev. E **65**, 046119 (2002).
[21] J. G. E. M. Fraaije, J. Chem. Phys. **99**, 9202 (1993); J. G. E. M. Fraaije, B. A. C. van Vlimmeren, N. M. Maurits, M. Postma, O. A. Evers, C. Hoffmann, P. Altevogt, and G. Goldbeck-Wood, *ibid.* **106**, 4260 (1997).
[22] S. M. Wood and Z.-G. Wang, J. Chem. Phys. **116**, 2289 (2002).
[23] G. H. Fredrickson and K. Binder, J. Chem. Phys. **91**, 7265 (1989).
[24] P. C. Hohenberg and J. B. Swift, Phys. Rev. E **52**, 1828 (1995).
[25] M. Nonomura and T. Ohta, J. Phys. Soc. Jpn. **70**, 927 (2001); J. Phys.: Condens. Matter **13**, 9089 (2001).
[26] D. A. Hajduk, S. M. Gruner, P. Rangarajan, R. A. Register, L. J. Fetters, C. Honeker, R. J. Albalak, and E. L. Thomas, Macromolecules **27**, 490 (1994).
[27] S. Sakurai, T. Momii, K. Taie, M. Shibayama, S. Nomura, and T. Hashimoto, Macromolecules **26**, 485 (1993).
[28] G. Floudas, R. Ulrich, U. Wiesner, and B. Chu, Europhys. Lett. **50**, 182 (2000).
[29] T. Hashimoto and N. Sakamoto, Macromolecules **28**, 4779 (1995).
[30] H. J. Dai, N. P. Balsara, B. A. Garetz, and M. C. Newstein, Phys. Rev. Lett. **77**, 3677 (1996).
[31] N. P. Balsara, B. A. Garetz, M. Y. Chang, H. J. Dai, M. C. Newstein, J. L. Goveas, R. Krishnamoorti, and S. Rai, Macromolecules **31**, 5309 (1998).
[32] N. P. Balsara, B. A. Garetz, M. C. Newstein, B. J. Bauer, and T. J. Prosa, Macromolecules **31**, 7668 (1998).
[33] S. A. Brazovskii, Sov. Phys. JETP **41**, 85 (1975).
[34] E. I. Kats, V. V. Lebedev, and A. R. Muratov, Phys. Rep. **228**, 1 (1993).
[35] J. Swift and P. C. Hohenberg, Phys. Rev. A **15**, 319 (1977).
[36] T. Ohta and K. Kawasaki, Macromolecules **19**, 2621 (1986).
[37] G. H. Fredrickson and E. Helfand, J. Chem. Phys. **87**, 697 (1987).
[38] M. S. Turner, M. Rubinstein, and C. M. Marques, Macromolecules **27**, 4986 (1994).
[39] V. E. Podneks and I. W. Hamley, JETP Lett. **64**, 617 (1996).
[40] J. L. Goveas and S. T. Milner, Macromolecules **30**, 2605 (1997).
[41] R. R. Netz, D. Andelman, and M. Schick, Phys. Rev. Lett. **79**, 1058 (1997).
[42] G. Wulff, Z. Kristallogr. Mineral. **34**, 449 (1901); C. Herring, Phys. Rev. **82**, 87 (1951); C. Rottman, and M. Wortis, Phys. Rep. **103**, 59 (1984).
[43] N. P. Balsara, C. M. Marques, B. A. Garetz, M. C. Newstein, and S. P. Gido, Phys. Rev. E **66**, 052802 (2002).
[44] R. Wickham (unpublished calculation). In the present work we use analytical expressions to compute the quantities appearing in Table I for all $f_A$, except for $N\Gamma_4(0,0)$. We obtain values for $N\Gamma_4(0,0)$ from Table I by interpolation which, given the approximate nature of the present theory, is sufficiently accurate.
[45] J. S. Rowlinson and B. Widom, *Molecular Theory of Capillarity* (Oxford University Press, New York, 1982).
[46] R. M. Hornreich, M. Luban, and S. Shtrikman, Phys. Rev. Lett. **35**, 1678 (1975).
[47] R. Holyst and M. Schick, J. Chem. Phys. **96**, 7728 (1992).
[48] P. M. Chaikin and T. C. Lubensky, *Principles of Condensed Matter Physics* (Cambridge University Press, Cambridge, 1995).
[49] K. Binder, Phys. Rev. A **29**, 341 (1984).
[50] Z.-G. Wang, J. Chem. Phys. **117**, 481 (2002).
[51] S. Koizumi, H. Hasegawa, and T. Hashimoto, Macromolecules **27**, 6532 (1994).
[52] C. Y. Ryu, M. E. Vigild, and T. P. Lodge, Phys. Rev. Lett. **81**, 5354 (1998); C. Y. Ryu and T. P. Lodge, Macromolecules **32**, 7190 (1999).